XLVII JORNADAS DE AUTOMÁTICA
CÓRDOBA 2026

Jornadas de Automática

Comparison of State-Space and LSTM-Based Virtual Temperature modelling in fuel cells.

Abiola, A O.*, Barragán A. J., Andújar, J M, Segura, F,
Centro de Investigación en Tecnología, Energía y Sostenibilidad (CITES), Universidad de Huelva, España

To cite this article: Abiola, A.O., Barragán A. J., Andújar, J.M., Segura, F., 2026. Comparison of State-Space and LSTM-Based Virtual Temperature modelling in fuel cells. Jornadas de Automática, 47.
https://doi.org/10.17979/ja-cea.2026.47.13863

Resumen

Este estudio compara enfoques basados en modelos de espacio de estados y redes Long Short-Term Memory (LSTM) para el sensado virtual de la temperatura de salida en pilas de combustible de membrana de intercambio protónico (PEMFC). Se recopilaron datos experimentales de corriente de pila, temperatura de entrada del agua de refrigeración y temperatura de salida del agua de refrigeración bajo condiciones dinámicas de operación. El modelo de espacio de estados se desarrolló mediante técnicas de identificación de sistemas, mientras que el modelo LSTM se entrenó utilizando un enfoque basado en aprendizaje secuencial de datos. Se evaluaron diferentes combinaciones de entradas mediante el error cuadrático medio (RMSE) y análisis de correlación. Los resultados mostraron que ambos métodos pudieron seguir el comportamiento térmico, aunque su desempeño dependió significativamente de la selección de entradas y de la observabilidad térmica.

Palabras clave: Pilas de Combustible PEM, Sensado Virtual de Temperatura, Modelado en Espacio de Estados, Long Short-Term Memory (LSTM), Identificación de Sistemas, Monitoreo Tolerante a Fallos.

Comparación entre modelos de espacio de estados y LSTM para la estimación virtual de temperatura en pilas de combustible PEM

Abstract

This study compares model-based state-space prediction and Long Short-Term Memory (LSTM) approaches for virtual outlet-temperature sensing in proton exchange membrane fuel cells (PEMFCs). Experimental data consisting of stack current, inlet cooling-water temperature, and outlet cooling-water temperature were collected under dynamic operating conditions. The state-space model was developed using system identification techniques, while the LSTM model was trained using a data-driven sequence-learning approach. Different input combinations were evaluated using root mean square error (RMSE) and correlation analysis. Results showed that both methods could track thermal behaviour, although their performance depended strongly on input selection and thermal observability. The LSTM demonstrated strong capability in learning nonlinear thermal dynamics, while the state-space approach provided improved physical interpretability.

Keywords: PEM Fuel Cells, Virtual Temperature Sensing, State-Space Modelling, Long Short-Term Memory (LSTM), System Identification, Fault-Tolerant Monitoring.

1. Introduction

Proton Exchange Membrane Fuel Cells (PEMFCs) require reliable thermal monitoring to ensure safe operation, efficiency, and durability (Abiola et al., 2023). Among the monitored variables, outlet cooling-water temperature is particularly important because it reflects the thermal state of the fuel cell stack and strongly influences performance, degradation, and system reliability. However, temperature sensors may fail due to drift, noise, aging, wiring problems, or harsh operating conditions. Attempts to install redundant physical sensors is not always practical because of economic cost, limited installation space, maintenance complexity, and system integration constraints. Consequently, virtual sensing techniques have emerged as attractive alternatives capable of

*Autor para correspondencia: abiodun.abiola@alu.uhu.es

providing backup or estimated measurements when physical sensors become unreliable or unavailable.(Ariza et al., 2023).

Virtual sensing can be achieved using different modelling approaches, broadly categorized into model-based and data-driven methods. Model-based approaches, such as state-space models (SSM), rely on system dynamics and physical interpretability, while data-driven methods such as Long Short-Term Memory (LSTM) networks learn nonlinear relationships directly from operational data. (Ignatenko et al., 2019), (Abiola et al., 2023).

Recent studies have highlighted the importance of comparing these modelling approaches to better understand their respective strengths and limitations in dynamic system prediction (Guffanti and Pavon, 2025). Furthermore, hybrid SSM-LSTM frameworks have demonstrated that state-space models offer interpretability, whereas LSTMs provide greater flexibility for capturing nonlinear and long-range temporal dependencies that are often difficult to represent using conventional state-space formulations (Vuong et al., 2025; Zheng et al., 2017). Motivated by these observations, this study compares state-space and LSTM-based virtual temperature sensing approaches when applied to hydrogen technologies such as PEM fuel cells with the aim to evaluate how model structure influences prediction accuracy. The contribution of this work is not the development of a new state-space or LSTM algorithm, but a systematic comparison of model-based and data-driven virtual temperature sensing approaches for PEM fuel cells under different predictor-variable configurations. The study further evaluates how predictor-variable selection influences model accuracy, and practical deployment considerations. The remainder of this paper is organized as follows. Section 2 presents the methodology to implement the state-space and LSTM modelling approaches as well as experimental setup. Section 3 discusses the model evaluation results and comparative analysis, while Section 4 summarizes the main conclusions for virtual temperature sensing in PEM fuel cells.

2. Methodology

To achieve the objectives of this study, state-space and LSTM neural network models were developed using experimental PEM fuel cell data and evaluated under different input-variable configurations. Stack current (I), stack voltage (V), and inlet cooling-water temperature (T_{in}), were considered as input variables, while outlet cooling-water temperature (T_{out}) was selected as the output variable. The resulting models were compared with the aim of assessing the influence of model structure on virtual temperature prediction accuracy. Model performance was assessed using the root mean square error (RMSE), mean absolute error (MAE) and maximum error. For each model, the experimental dataset was divided into training and testing subsets, with 70% of the data used for model identification and parameter estimation, while the remaining 30% was reserved for model evaluation.

2.1. State space model

A dynamic system can be represented using a state-space model, in which the system is described by input variables, output variables, and a set of internal state variables that capture its dynamic behaviour over time (Ignatenko et al., 2019). The general discrete-time state-space formulation is given by (1) and (2).

$$x(k+1) = Ax(k) + Bu(k) \quad (1)$$
$$y(k) = Cx(k) + Du(k) \quad (2)$$

where:

- x represents the state vector,
- u represents the input vector,
- y represents the predicted output vector
- k represents sampling time
- A is the state-transition matrix describing the internal system dynamics,
- B is the input matrix describing the influence of the inputs on the states,
- C is the output matrix relating the states to the measured output,
- D is the direct feedthrough matrix representing direct input–output coupling.

The values of the state-space matrices A, B, C and D were determined from experimental data using the Numerical algorithms for Subspace State Space System Identification (N4SID) method (MathWorks, 2026). For each input-variable combination, a parameter sweep was performed by varying the model order (1–8), estimation focus (prediction or simulation), subspace weighting method (Auto, CVA, MOESP, and SSARX), and stability constraint settings. The optimal configuration was selected based on the lowest validation RMSE. The optimum configurations for each input-variable combination are summarized in Table 3. Stability enforcement was retained for all identified models to ensure physically realistic and bounded thermal behaviour. The identified state-space matrices A, B, C, and D were subsequently used to recursively estimate the outlet cooling-water temperature from the selected input variables.

2.2. Long short-term memory neural network (LSTM)

Figure 1 illustrates the internal architecture of the LSTM network for virtual temperature prediction using data based approach (Abiola et al., 2023). Unlike conventional recurrent neural networks, the LSTM structure contains memory cells and gating mechanisms that enable the network to retain or discard information over time.

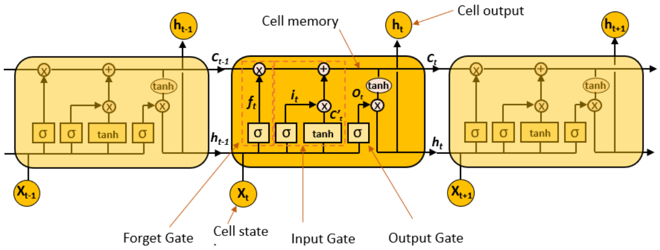

Figure 1: Concept of LSTM Neural Network

The equations for each cell gate and state are the following:

$$Forget\ Gate: f_t = \sigma\left(W_f . \left[h_{t-1,} x_t\right] + b_f\right) \quad (7)$$

$$Input\ Gate: i_t = \sigma\left(W_i . \left[h_{t-1,} x_t\right] + b_i\right) \quad (8)$$

$$Output\ Gate: O_t = \sigma\left(W_o . \left[h_{t-1,} x_t\right] + b_o\right) \quad (9)$$

$$Candidate\ valve\ C'_t = \tanh\left(W_c . \left[h_{t-1,} x_t\right] + b_c\right) \quad (10)$$

$$Cell\ State: C_t = f_t * C_{t-1} + i_t * C'_t \quad (11)$$

$$Hidden\ State: h_t = \sigma_t * \tanh(C_t) \quad (12)$$

where:

t is the time step

b, is a bias added for each gate

W_f , W_i *and* W_o are the weight of each gate

h_t and h_{t-1}, *are* the output for the hidden states in time steps t and t-1 respectively

x_t, *is* the input at time t

σ is the sigmoid activation function

Stack current (I), stack voltage (V), inlet cooling-water temperature (T_{in}), and their combinations were used as network inputs, while outlet cooling-water temperature (T_{out}) was used as the target output. The LSTM model was developed using a 70%:30% training-testing data split, consistent with the state-space modelling approach to enable a fair comparison.

The LSTM architecture consisted of a sequence input layer, a single LSTM layer, a fully connected layer, and a regression output layer. The LSTM layer was configured with *OutputMode = sequence*, enabling prediction of the outlet temperature at every sampling instant. The input data were arranged as complete normalized time sequences rather than fixed-length sliding windows; therefore, the effective sequence length corresponded to the number of samples in the training or testing dataset.

Hyperparameter optimization was performed independently for each input-variable combination by varying the number of hidden units (50–200), initial learning rate (0.002–0.1), and mini-batch size. The final models were trained using the Adam optimizer with a maximum of 100 epochs, a gradient threshold of 1, a piecewise learning-rate schedule, a learning-rate drop factor of 0.5, and a learning-rate drop period of 50 epochs. The optimum hidden units, learning rate, and mini-batch size selected for each input combination are summarized in Table 3

2.3. *Experimental Data Acquisition*

Experimental data were collected from a PEM fuel cell system shown in Figure 2 consisting of a 10-cell stack with an active area of 220 cm² per cell. Details of the set up are shown in Table 1. The fuel cell was operated using commercial dry hydrogen under dynamic loading conditions in order to generate varying thermal responses suitable for virtual temperature sensing analysis.

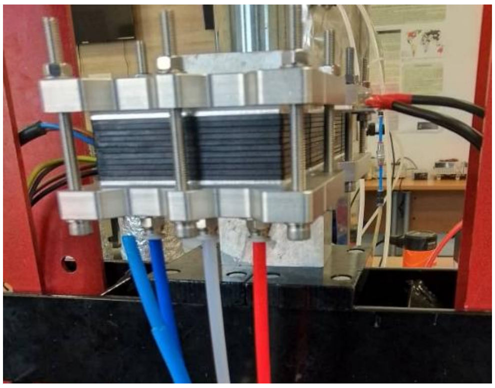

Figure 2: PEM fuel cell and test bench used in the study.

The operating condition of the stack follows the current demand with hydrogen inlet pressure between 0.2 and 0.4 bar, air inlet pressure between 0.1 and 0.2 bar, stack inlet air flow rate between 14 and 51 L/min, and air relative humidity between 70 and 80%. The cooling system was operated under variable flow conditions to capture the influence of thermal boundary variations on outlet temperature dynamics. The cooling-water flow rate varied between 0.3125 and 3.17 L/min during the experiment to prevent stack overheating. Although coolant flow rate influences PEMFC thermal behaviour, it was not included as a model input because the study focused on evaluating the predictive capability of stack current, voltage, and inlet cooling-water temperature. The effect of coolant-flow variations was therefore implicitly reflected in the measured thermal response.

Table 1: Experimental set-up

Parameter	Value	Measurement Device
Number of Cells	10 cells	-
Active Area	220 cm^2	-
Air pressure	0.1 - 0.2 bar	Festo SFAB
Air flow	14 - 51 L/min	
Air Humidity	70 - 80%	Texense PTH CAN
Hydrogen Pressure	0.2 - 0.4 bar	Alicat M Series
Hydrogen Flow	0 – 16 slpm	
Hydrogen Humidity	0 % (dry hydrogen)	Trican HTD2800
Current	0 – 220 A	B&K 8415B
Voltage	0 to 10 V	
Temperature	22 to 60 ºC	WIKA TF35

Data were acquired at a sampling interval of 1 s using LabVIEW® software and a National Instruments USB-6218 data-acquisition device.

These data were continuously recorded under transient operating conditions to generate datasets containing both electrical and thermal dynamic behaviour. This is shown in Figure 3 and Figure 4. These data were subsequently used for the development and evaluation of SSM and LSTM-based virtual temperature sensing approaches.

For the case of LSTM, the experimental data were pre-processed before model development and evaluation. Signal normalization using 0–1 scaling was applied to improve numerical stability and training performance.

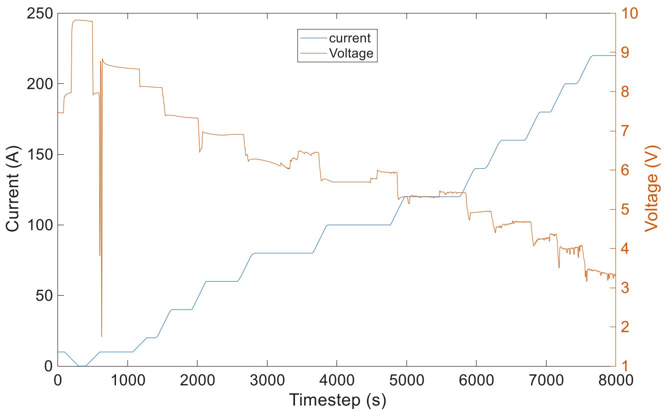

Figure 3: Experimental data showing variation of current and voltage.

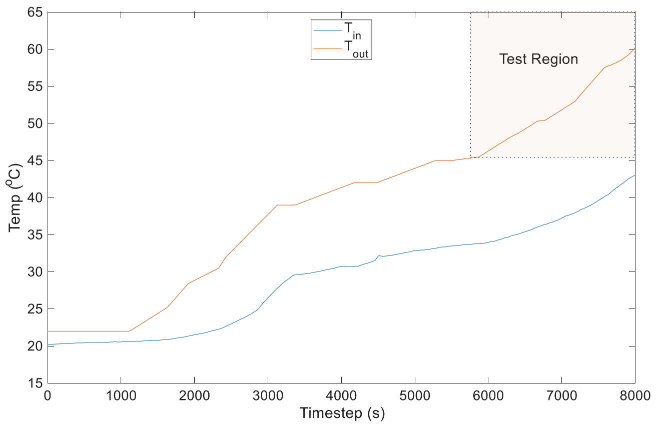

Figure 4: Experimental data showing variation of inlet and outlet cooling water temperature as well as the test region.

Figure 4 also shows a test region corresponding to the testing of 30% dataset used for validating the state-space and LSTM virtual temperature prediction models.

2.4. Analysis of Input and Output Relationships

In state-space system identification, the objective is not to utilize all the available inputs data, but rather to select the most dynamically and physically observable variables capable of representing the system behaviour. Figure 5 presents the correlation matrix to evaluate the statistical relationship between the input and output variables of the fuel cell.

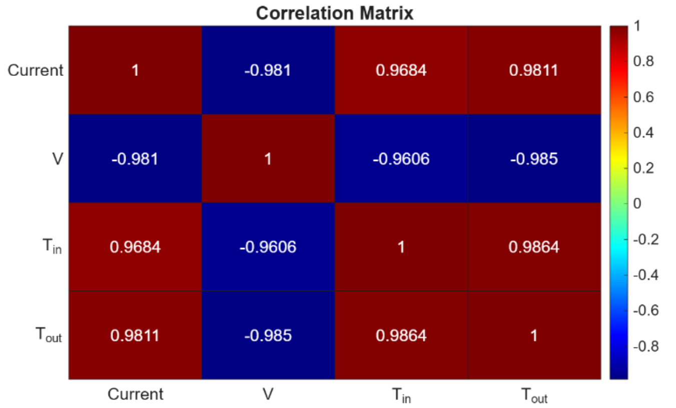

Figure 5: Correlation matrix of experimental data

Although the correlation analysis demonstrated strong statistical relationships between the measured variables and outlet temperature, such correlation alone was not considered sufficient for final input selection. Therefore, different input configurations consisting of I, V, T_{in} , [I + V], [I + T_{in}], [V + T_{in}], [I +V + T_{in}] were selected and evaluated using both the state-space and LSTM-based virtual temperature prediction models.

3. **Results**

Table 2 presents the values of the matrices for modelling in state space model for different input combinations. The state-transition matrix (A) remained close to unity (0.9982–1.0000) for all models, indicating strong thermal memory and slow PEMFC thermal dynamics. Matrix (B) describes the influence of the selected input variables on the thermal state, with multi-input models assigning separate coefficients to current, voltage, and inlet cooling-water temperature. Matrix (C) relates the thermal state to the measured outlet temperature, while the zero-valued (D) matrix indicates that outlet temperature evolves through the system dynamics rather than responding instantaneously to input changes. Under prolonged constant-current operation, the virtual sensor would initially predict a gradual temperature increase; however, the rate of temperature rise would be expected to decrease as heat removal through the cooling circuit balances heat generation within the stack.

Table 2: Matrices obtained for different combinations of input in the state space model

Input	**A**	**B**	**C**	**D**
I	1	7.7357×10^{-5}	0.7071	0
V	1	-4.7627×10^{-4}	-0.7071	0
T_{in}	1	1.4467×10^{-6}	-196.5259	0
[I + V]	0.9999	$[0.0716 \quad 0.9388] \times 10^{-3}$	0.7071	0
[I + T_{in}]	0.9984	$[-0.0002 \quad -0.0028]$	-0.7065	0
[V + T_{in}]	0.9982	$[0.3373 \quad -0.7928] \times 10^{-4}$	−34.7640	0
[I +V + T_{in}]	1	$[-0.0003 \quad -0.0053 \quad 0.0038]$	-0.7067	0

3.1. Model Evaluation and comparison

Table 3 summarizes the optimal state-space identification settings and LSTM hyperparameters obtained for each input-variable combination. All optimum state-space models resulted in first-order structures, indicating that the dominant PEMFC thermal dynamics can be represented by low-order models. Prediction-focused estimation and MOESP weighting were selected in most cases. For the LSTM models, optimum hyperparameters varied across input combinations, with hidden units ranging from 50 to 150 and learning rates from 0.0030 to 0.022, highlighting the need for independent tuning.

Table 3: Final SSM and LSTM model configurations obtained after parameter optimization

Model Input	**SSM**				**LSTM**			
	Order	**Focus**	**Weight**	**Stable**	**Hidden Units**	**Learning Rate**	**Epoch**	**Mini Batch Size**
I	1	Prediction	MOESP	True	100	0.022	100	1
V	1	Prediction	MOESP	True	50	0.0080	100	1
T_{in}	1	Prediction	Auto	True	100	0.0086	100	1
[I + V]	1	Prediction	MOESP	True	150	0.0040	100	1
[I + T_{in}]	1	Simulation	MOESP	True	50	0.0030	100	1
[V + T_{in}]	1	Prediction	SSARX	True	100	0.0054	100	1
[I + V + T_{in}]	1	Prediction	MOESP	True	150	0.0092	100	1

The predictive performance of the resulting models is presented in Figure 6. The plots correspond to the test region of Figure 4. In each case, only the variables indicated in the subplot title were supplied to the model as inputs, while the remaining measured variables were excluded from the input vector rather than being held constant. For example, in case (a), stack current was the only predictor variable used by the model, whereas voltage and inlet cooling-water temperature were not included as model inputs. Similarly, cases (b) up to (g) were generated using the corresponding input combinations shown in each subplot.

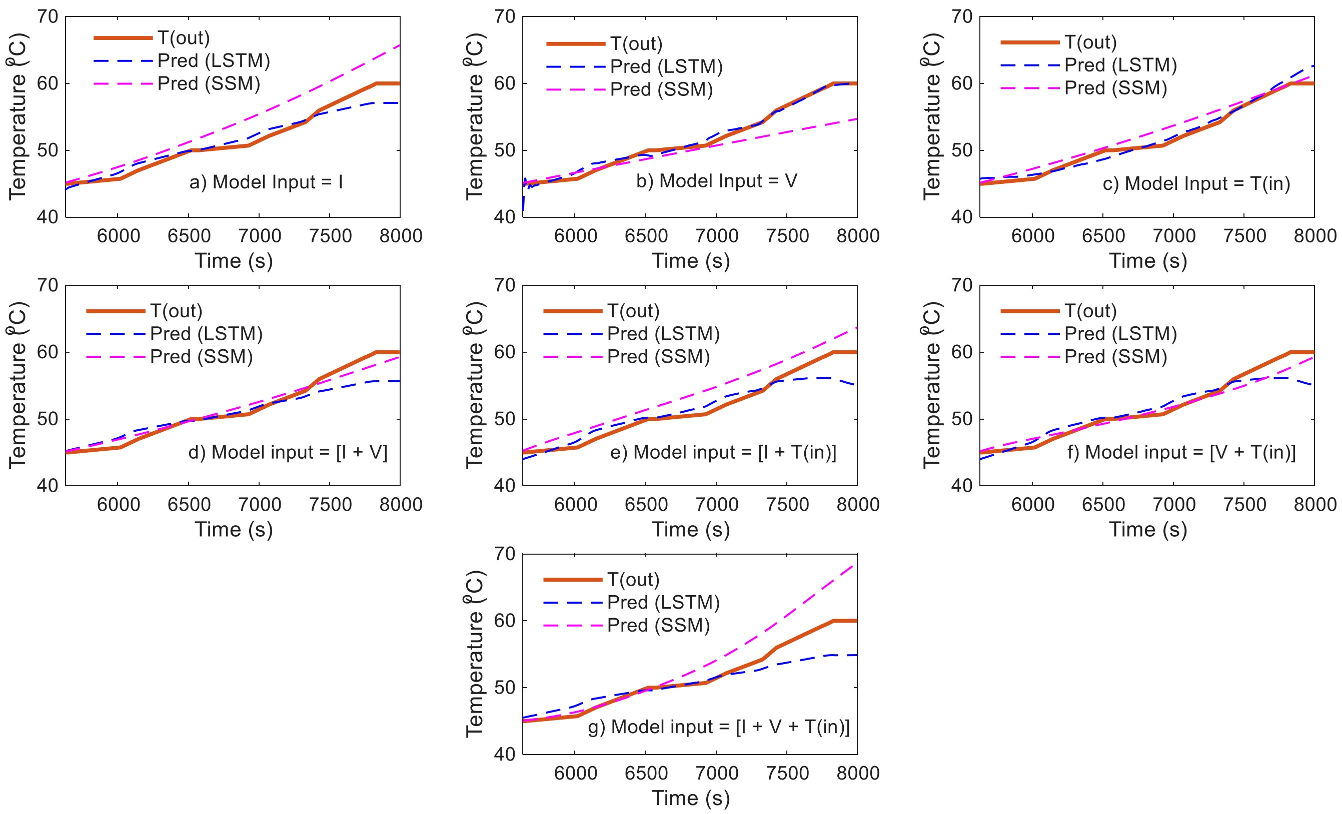

Figure 6: Performance evaluation of models (LSTM and SSM).

Table 4 compares the prediction performance of the SSM and LSTM models using RMSE, MAE, and maximum error (MaxErr) for different input combinations as shown in Figure 6.

For all single-input configurations, the LSTM achieved lower RMSE, MAE, and maximum error values than the SSM, indicating superior prediction accuracy across individual predictor variables. Among the single-input configurations, T_{in} provided the best performance for both approaches, yielding RMSE values of 0.8740 and 1.2729 for the LSTM and SSM, respectively. This indicates T_{in} contains significant information regarding the thermal state and boundary conditions of the fuel-cell system.

Table 4: Comparison of prediction errors between SSM and LSTM models

Model Input	SSM			LSTM		
	RMSE	**MAE**	**MaxErr**	**RMSE**	**MAE**	**MaxErr**
I	3.0651	2.7423	5.7414	1.4555	0.9380	2.9110
V	2.6557	1.8679	5.9701	0.9432	0.3938	1.2717
T_{in}	1.2729	1.0820	2.4679	0.8740	0.6191	2.6287
[I + V]	0.8997	0.7700	1.88141	1.6897	1.2992	3.4342
[I + T_{in}]	2.3674	2.2378	3.6829	1.7906	1.2086	4.9057
[V + T_{in}]	1.0742	0.8240	2.3163	1.4111	1.1390	2.3867
[I + V + T_{in}]	3.2399	2.3000	8.7140	2.2597	1.5777	5.1489

For multi-input models, the best SSM performance was obtained using [V+T_{in}] and has RMSE = 1.0742 and MAE = 0.8240. However, the best LSTM performance was achieved using voltage alone whose RMSE = 0.9432 and MAE = 0.3938. The [I+V+T_{in}] configuration increased the error in both models, suggesting redundancy and possible multicollinearity among the predictor variables.

The PEM fuel-cell thermal behaviour results from strongly coupled electrochemical and thermal processes. Consequently, multivariable models can provide improved observability by simultaneously capturing heat-generation effects through voltage and current measurements and thermal boundary conditions through inlet cooling-water temperature. However, improved observability does not necessarily translate into lower prediction error, as additional variables may introduce redundancy and multicollinearity. This behaviour was observed for the [I+V+T_{in}] configuration, whereas the superior performance of the [V+T_{in}] state-space model suggests that combining complementary electrochemical and thermal information can improve outlet-temperature estimation.

The validation results correspond to the final 30% of the experimental dataset, which is characterized by a predominantly increasing temperature profile. Consequently, the reported metrics quantify model performance within this operating region and may not fully represent behavior under cooling phases, steady-state operation, or independent experimental datasets. Future work will investigate broader validation scenarios, including cross-validation and independent experimental runs.

Overall, the LSTM demonstrated superior prediction accuracy across most input combinations, while the SSM achieved competitive performance when physically meaningful thermal variables were combined. These findings support the feasibility of both approaches for virtual temperature sensing during outlet-temperature sensor failure.

To verify implementation repeatability, each LSTM configuration was retrained five times using identical training conditions. A fixed random seed was specified prior to network initialization, ensuring identical initialization weights, bias values, data shuffling, and optimization sequences across runs. Identical prediction metrics were obtained in all repetitions, yielding a standard deviation of zero for the reported RMSE values. This confirms reproducibility under the selected training configuration. Residual analysis showed bounded errors with no significant systematic drift.

3.2. Model Selection for Industrial Deployment

For industrial applications as regards hydrogen technologies, the selection of predictor variables for virtual temperature sensing should not be based solely on RMSE, but also on the ability of the model to remain reliable under changing operating, thermal, and degradation conditions.

Table 5 shows that the lowest LSTM prediction error (RMSE = 0.9432), was obtained using voltage alone whereas the lowest SSM model prediction error (RMSE = 1.0742). was achieved using the combination of voltage and inlet cooling-water temperature.

Table 5: Optimal predictor variables obtained from model analysis

Model	**SSM**	**Model Input**
SSM	1.0742	[V + T_{in}]
LSTM	0.9432	V

Although voltage alone provided the highest LSTM accuracy, this does not necessarily make it the preferred choice for practical deployment. Voltage contains valuable electrochemical and thermal information, allowing accurate temperature estimation within the dataset investigated. However, the superior performance of the [V + T_{in}] in SSM indicates that combining electrochemical information with thermal boundary-condition information improves system observability. While adding T_{in} did not improve the LSTM results in this study, multi-variable models are generally more robust because they are less dependent on a single measurement and better able to accommodate changes in operating conditions and system degradation. Consequently, voltage-only LSTM models may be suitable for low-cost virtual sensing, whereas [V + T_{in}] models may offer greater reliability for industrial applications.

4. Conclusion

This study compared state-space modelling (SSM) and Long Short-Term Memory (LSTM) networks for virtual outlet-temperature prediction in PEM fuel cells using different input-variable combinations. The results showed that input selection significantly affects model accuracy, with the LSTM achieving the best performance using voltage alone (RMSE = 0.9432) and the SSM achieving its highest accuracy using voltage and inlet cooling-water temperature (RMSE = 1.0742). The findings highlight the importance of combining electrochemical and thermal information to improve system observability and fault-tolerant temperature estimation. For practical deployment, SSMs are attractive for Industrial and embedded controllers due to their simplicity and low computational requirements, whereas LSTM models are preferred when maximum prediction accuracy is required and greater computational resources are available. Future work involves further testing of the models with additional experimental data.

Acknowledgments

This work has been partially carried out thanks to the support of (1) Grant Ref: PID2020-116616RB-C31 and (2) Triple-M Ref.: EPIT0872023-UHU.

References

Abiola, A., Manzano, F.S., Andújar, J.M., 2023. A Novel Deep Reinforcement Learning (DRL) Algorithm to Apply Artificial Intelligence-Based Maintenance in Electrolysers. Algorithms 16, 541. https://doi.org/10.3390/a16120541

Ariza, E., Correcher, A., Vargas-Salgado, C., 2023. PEMFCs Model-Based Fault Diagnosis: A Proposal Based on Virtual and Real Sensors Data Fusion. Sensors 23, 7383. https://doi.org/10.3390/s23177383

Guffanti, D., Pavon, W., 2025. MultivariateSystem Identification of Differential Drive Robot: Comparison Between State-Space and LSTM-Based Models. Sensors 25, 5821. https://doi.org/10.3390/s25185821

Ignatenko, V., Yudintsev, A., Lyapunov, D., 2019. Application of State-Space Method for Control System Analysis, in: 2019 International Siberian Conference on Control and Communications (SIBCON). Presented at the 2019 International Siberian Conference on Control and Communications (SIBCON), IEEE, Tomsk, Russia, pp. 1–5. https://doi.org/10.1109/SIBCON.2019.8729658

MathWorks, 2026. System Identification Toolbox User's Guide. The MathWorks, Inc., Natick, Massachusetts, USA.

Vuong, V.-D., Nguyen, L.-H., Goulet, J.-A., 2025. Coupling LSTM neural networks and state-space models through analytically tractable inference. International Journal of Forecasting 41, 128–140. https://doi.org/10.1016/j.ijforecast.2024.04.002

Zheng, X., Zaheer, M., Ahmed, A., Wang, Y., Xing, E.P., Smola, A.J., 2017. State Space LSTM Models with Particle MCMC Inference. https://doi.org/https://doi.org/10.48550/arXiv.1711.11179